RESEARCH ARTICLE

ADVANCED
ENERGY & SUSTAINABILITY
RESEARCH
Open Access

www.advenergysustres.com

Unraveling the Impact of Combined NaF/RbF Postdeposition Treatments on the Deeply Buried Cu(In,Ga)Se₂/Mo Thin-Film Solar Cell Interface

Jakob Bombsch,* Enrico Avancini, Romain Carron, Evelyn Handick, Raul Garcia-Diez, Claudia Hartmann, Roberto Félix, Daniel Abou-Ras, Shigenori Ueda, Regan G. Wilks, and Marcus Bär*

Cu(In,Ga)Se₂ (CIGSe) is a promising absorber material for thin-film photovoltaic devices. A key procedure to achieve high efficiencies is the application of alkali fluoride postdeposition treatments (PDT) of the CIGSe surface. While the effects of the PDT on the directly impacted CIGSe front surface have been subject to extensive studies, less is known about the impact on the deeply buried CIGSe/Mo interface. Exposing the CIGSe absorber backside by stripping it off the Mo back contact allows to use surface-sensitive photoelectron spectroscopy to study the chemical and electronic structure of this interface in unprecedented detail. CIGSe/Mo stacks prepared using NaF only and combined NaF/RbF (with optimal and excess amount of RbF) PDT are studied. Rb is detected accumulating at the backside of the RbF-treated CIGSe absorbers in conjunction with a depletion of Na. The exposed CIGSe backsides display a Cu-deficient surface region, with increased presence of Rb correlating with a decreased Cu content. Rb appears to be incorporated into the Cu-deficient absorber region as previously detected on the front surface. However, in contrast to the front surface, no distinct, secondary Rb—In—Se-type phase is found at the back surface.

1. Introduction

Techniques to incorporate alkali elements into Cu(In,Ga)Se₂ (CIGSe) absorbers are widely used in the manufacture of highly efficient chalcopyrite solar cells. Na is widely supplied via diffusion from the soda lime glass (SLG) into the CIGSe absorber. Alternatively, Na can also be provided via a postdeposition treatment (PDT), in cases where diffusion from the SLG is not possible (i.e., when using alternative Na-free substrates) or desired.[1] The heavier alkali elements K, Rb, and Cs are commonly introduced through an alkali fluoride PDT.[2,3] In fact, it has been shown recently that the use of the heavier alkalis K,[2] Rb,[4] and Cs[5,6] has led to a significant increase in solar cell performance, reported to be due to an increase in the open-circuit voltage (V_{OC}) and the fill factor (FF).[1,4,7] In addition, these PDTs allow the use of thinner CdS buffer layers, which reduces parasitic absorption losses in the buffer, increasing the short-circuit current (J_{SC}).[7]

J. Bombsch, E. Handick, R. Garcia-Diez, C. Hartmann, R. Félix, R. G. Wilks, M. Bär
Interface Design
Helmholtz-Zentrum Berlin für Materialien und Energie GmbH
Berlin 12489, Germany
E-mail: jakob.bombsch@helmholtz-berlin.de;
marcus.baer@helmholtz-berlin.de

E. Avancini, R. Carron
Laboratory for Thin Films and Photovoltaics
Empa-Swiss Federal Laboratories for Materials Science and Technology
Dübendorf 8600, Switzerland

The ORCID identification number(s) for the author(s) of this article can be found under https://doi.org/10.1002/aesr.202100101.

E. Avancini
Faculty of Science and Technology
Free University of Bozen-Bolzano
Bolzano 39100, Italy

D. Abou-Ras
Department for Structure and Dynamics of Energy Materials
Helmholtz-Zentrum Berlin für Materialien und Energie GmbH
Berlin 14109, Germany

S. Ueda
NIMS Synchrotron X-ray Station at SPring-8
National Institute for Materials Science (NIMS)
1-1-1 Kouto, Sayo, Hyogo 679-5148, Japan

S. Ueda
Research Center for Advanced Measurement and Characterization
NIMS
1-2-1 Sengen, TsukubaIbaraki, 305-0047, Japan

S. Ueda
Research Center for Functional Materials
NIMS
1-1 Namiki, TsukubaIbaraki, 305-0044, Japan

However, the exact mechanisms leading to the V_{OC} and FF improvements are still not fully understood.[8,9]

The heavy alkali PDTs impact the chemical[1,3,7,10–12] and electronic[13,14] structure of the CIGSe front surface region, e.g., by formation of an alkali—In—Se compound, which has been reported in the cases of using K[10] and Rb,[11,12] as well as a heavy alkali PDT-related reduction of the Cu surface content.[1,3,7] Apart from their impact on the surface region, heavy alkalis also diffuse along the grain boundaries into the CIGSe absorber affecting bulk properties.[8,15,16] Therefore, an accumulation of heavy alkalis can be found at the CIGSe/Mo back interface.[7,15,17] This might be related to the finding that a pronounced RbF PDT leads to the formation of a charge carrier transport barrier at one of the cell interfaces,[18] even though this barrier was suggested to be located at the CIGSe frontside because it can be reduced by etching the absorber surface.[18] To derive a more detailed picture of the impact of the Rb on the chemical and electronic CIGSe/Mo structure, we performed a photoemission study of the electronic and chemical properties of this deeply buried interface as a prerequisite for a further knowledge-based process optimization.

A previously used method to study the CIGSe/Mo back interface by surface-sensitive photoelectron spectroscopy is to strip off the CIGSe absorber from the Mo back contact to expose the CIGSe backside and Mo contact surfaces.[19–21] To examine the impact of a NaF(/RbF) PDT on the CIGSe/Mo back interface, we combine this approach with excitation energy-dependent photoelectron spectroscopy to study the CIGSe backside and respective Mo counterpart of samples that underwent NaF (only) and combined NaF/RbF PDT with different RbF evaporation rates: the standard rate that is optimized for high-efficiency solar cells and a RbF evaporation rate increased by a factor of approximately two. The latter treatment is known to significantly deteriorate solar cell properties by decreasing the open-circuit voltage (V_{OC}) and the fill factor (FF).[7] Previously, we investigated the chemical and electronic structure of the front surface of the same samples (see Bombsch et al.[11] and Experimental Section), finding Rb in two distinct chemical environments which we attributed to a Rb—In—Se-type phase and to Rb incorporated in the Cu-deficient CIGSe surface region.[11]

2. Results and Discussion

The survey spectra, measured with different excitation energies (1.5 (Al K$_\alpha$), 2, and 6 keV) shown in Figure S1, Supporting Information, indicate the presence of all CIGSe elements at the CIGSe backside. Furthermore, oxygen- and carbon-related signals were detected, which might be attributed to surface adsorbates resulting from unavoidable residual contamination, despite the cleavage being performed in an inert atmosphere (liquid nitrogen) and our following precautions taken to reduce

environmental exposure as much as possible as discussed in the Experimental Section. The inclusion of some of these elements into the bulk of the absorber (during deposition) is also a possible scenario. A detailed analysis of the presence of carbon and possible related impacts on our evaluation can be found in the Supporting Information section "Presence of Carbon" including Figure S2 and S3, Supporting Information. The survey scans show no indication of Mo on the CIGSe backside; however, detailed measurements of the Se 3s/Mo 3d region with 1.3 keV (Mg K$_\alpha$) (Figure S4, Supporting Information) reveal small Mo signals; the derived Mo/Se ratios range between 0.002 ($\pm$0.002) and 0.007 ($\pm$0.003) for the different samples. These values are equivalent to a MoSe$_2$ monolayer coverage of the CIGSe backside between approximately 1($\pm$1)% and 5($\pm$1)%. The pronounced surface sensitivity of Mg Kα measurements combined with the high photoionization cross section of the Mo 3d line[22] gives this approach a high sensitivity for detecting possible Mo remnants. The low Mo content indicates a successful strip-off, which is corroborated by the fact that no large Mo clusters can be seen in complementing energy-dispersive X-ray spectroscopy (EDX) maps (see section "Quality of stripped off sample surfaces" including Figure S5, S6, and S7, Supporting Information, for detailed discussion). This agrees with the fact that the strip-off method has been shown to be suitable to expose the absorber/substrate interface in chalcopyrite-based solar cells as previously reported.[19–21]

To thoroughly examine the absorbers, chemical composition, the shallow core levels of Rb 3d, Ga 3p, Cu 3p, Se 3d, Ga 3d, and In 4d were analyzed in detail. Their proximity in binding energy results in similar inelastic mean free paths (IMFPs) of the photoelectrons and thus the corresponding line intensities are affected very similarly by the presence of any surface adsorbates. Also, the intensities only need to be corrected by the respective photoionization cross sections when used for quantification (see Experimental Section for details). Furthermore, the relatively narrow natural line width of the Rb 3d, Se 3d, Ga 3d, and In 4d core levels increases the sensitivity to differentiate between different chemical species.[23] Close inspection of this spectral region revealed low-intensity I 4d signals in the case of the 2 keV hard X-ray photoelectron spectroscopy (HAXPES) data (Figure S8, Supporting Information), which we attribute to sample contamination during sample preparation, transport, storage, or mounting and assume to have negligible impact on quantification.

The Rb 3d, Ga 3p, Cu 3p (In 4p signals were subtracted; see Figure S9, Supporting Information), Na 2s, Se 3d, Ga 3d, and In 4d HAXPES spectra of the different absorber backsides are shown in **Figure 1** along with the fit results. All peak positions obtained from the fit can be found in Table S1, Supporting Information, and the respective 2 and 1.3 keV (Mg K$_\alpha$) spectra are shown in Figure S10 and S11, Supporting Information.

R. G. Wilks, M. Bär
Energy Materials In-Situ Laboratory Berlin (EMIL)
Helmholtz-Zentrum Berlin für Materialien und Energie GmbH
Berlin 12489, Germany

M. Bär
Department X-ray Spectroscopy at Interfaces of Thin Films
Helmholtz-Institute Erlangen-Nürnberg for Renewable Energy (HI ERN)
Berlin 12489, Germany

M. Bär
Department of Chemistry and Pharmacy
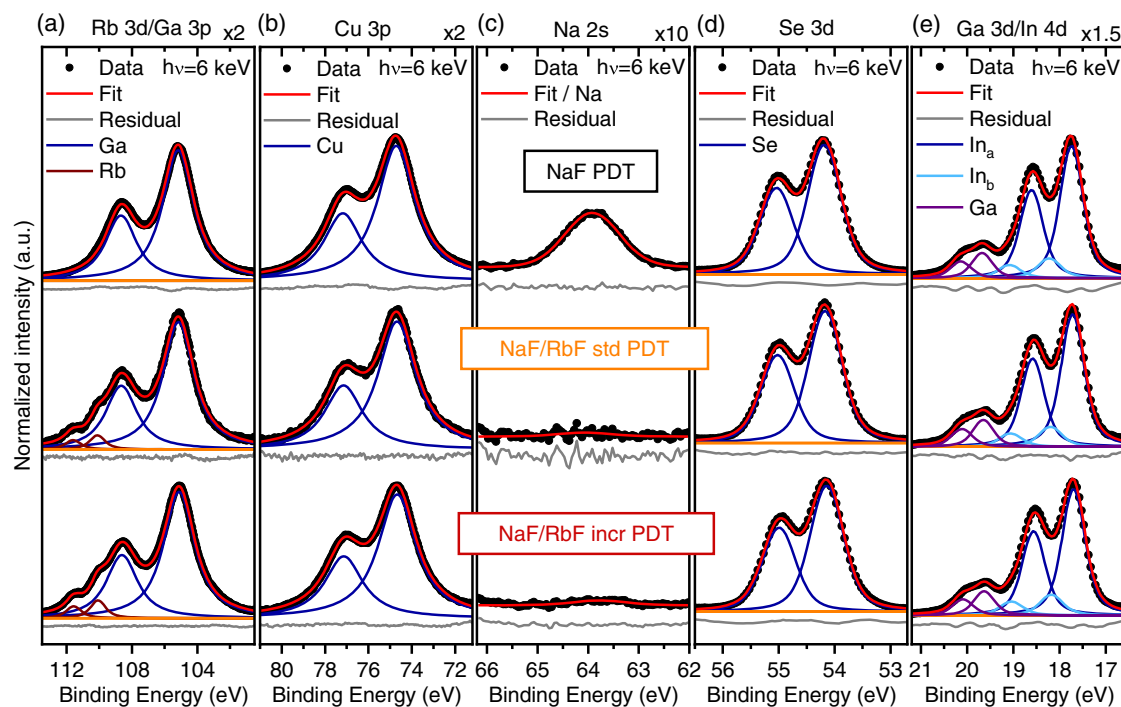Friedrich-Alexander-Universität Erlangen-Nürnberg
Erlangen 91054, Germany

Figure 1. HAXPES (6 keV) spectra of the backside of CIGSe samples, stripped off their substrates after undergoing a NaF PDT (top row spectra), combined NaF/RbF PDT as used for high-performance devices (middle row spectra), and combined NaF/RbF PDT with an increased RbF evaporation rate (bottom row spectra). a) Rb 3d/Ga 3p, b) Cu 3p, c) Na 2s, d) Se 3d, and e) Ga 3d/In 4d peaks are displayed. Data are shown with a linear background subtracted. Respective fits using pairs of Voigt profiles to represent the respective doublets are displayed along the data as well as the respective residuals. The Rb 3d/Ga 3p, Cu 3p, Na 2s, and Ga 3d/In 4d spectra are magnified by a factor given at the top right of the respective graphs for better visibility.

Except for the In 4d peak, all photoemission lines can be fitted with one component (note that each p or d state appears as a doublet due to the spin—orbit splitting), which is assigned to the chemical structure of CIGSe in the cases of Ga, Cu, Se, and In (In$_a$). An additional In species (In 4d component In$_b$) at slightly higher binding energies than the main CIGSe phase[24] is required for all samples to obtain a reasonable fit. Previously, we have attributed this component to In—O bonds[11] in agreement with the O 1s signal visible in the respective survey spectra (see Figure S1, Supporting Information, and discussed earlier). The data further show that after application of combined NaF/RbF PDT, Rb is present at the backside of the absorber, and the amount of Na is strongly reduced. The presence of Na and Rb at the back surface is in agreement with the previous finding that alkali metals tend to accumulate at the front and back surfaces of the CIGSe absorbers.[1,7] The detected Rb-induced reduction of Na is a widely recognized phenomenon[3,7] that can be explained by an ion exchange mechanism, details of which are still subject to vivid discussion.[15,25,26]

Only one kind of Rb is detected at the absorber backside, which is in contrast to our findings at the frontside of the same absorbers, where we recently detected two different Rb species, which we assigned to a Rb—In—Se-type compound and Rb incorporated in the Cu-deficient CIGSe surface region, respectively.[11] The binding energy of the detected backside Rb species of (110.1 ± 0.1) eV for Rb 3$d_{5/2}$ matches the binding energy of the latter.[11] This leads us to the conclusion that Rb diffuses to the CIGSe backside without forming a Rb—In—Se-type phase there. The formation of large amounts of RbInSe$_2$ at the absorber backside is not likely, as it would introduce substantial strain in the CIGSe lattice constraint by the contact to the Mo layer. In contrast, at the absorber frontside (where a Rb—In—Se-type compound could be identified[11]) this strain can easily be accommodated by the free surface.

Provided that liquid nitrogen does not dissolve Rb species or Rb-containing compounds during the stripping process, we conclude that no secondary Rb—In—Se-type compound is present at the absorber backside.

To obtain depth-dependent quantitative insights into the material, we calculated the stoichiometry (i.e., the [Ga]/([Ga]+[In]) (GGI), [Cu]/([Ga]+[In]) (CGI), [Rb]/([Cu]+[In]+[Ga]+[Se]), and [Na]/([Cu]+[In]+[Ga]+[Se]) ratios) from the photoemission spectra (shown in Figure 1, S10–S14, Supporting Information) measured with different excitation energies. Due to the resulting different photoelectron IMFPs, the respective ratios represent information integrated over different distances from the surface (see Experimental Section for further explanation). In **Figure 2**, we plot the resulting ratios versus their respective IMFP. In addition, we display corresponding CIGSe frontside data[11] of the respective samples for comparison. The calculated backside GGI is somewhat increased (in particular for large IMFPs), when comparing it with the frontside and increases marginally for lower IMFPs, indicating a slight Ga enrichment (on this depth scale) toward the back surface in agreement with the applied Ga
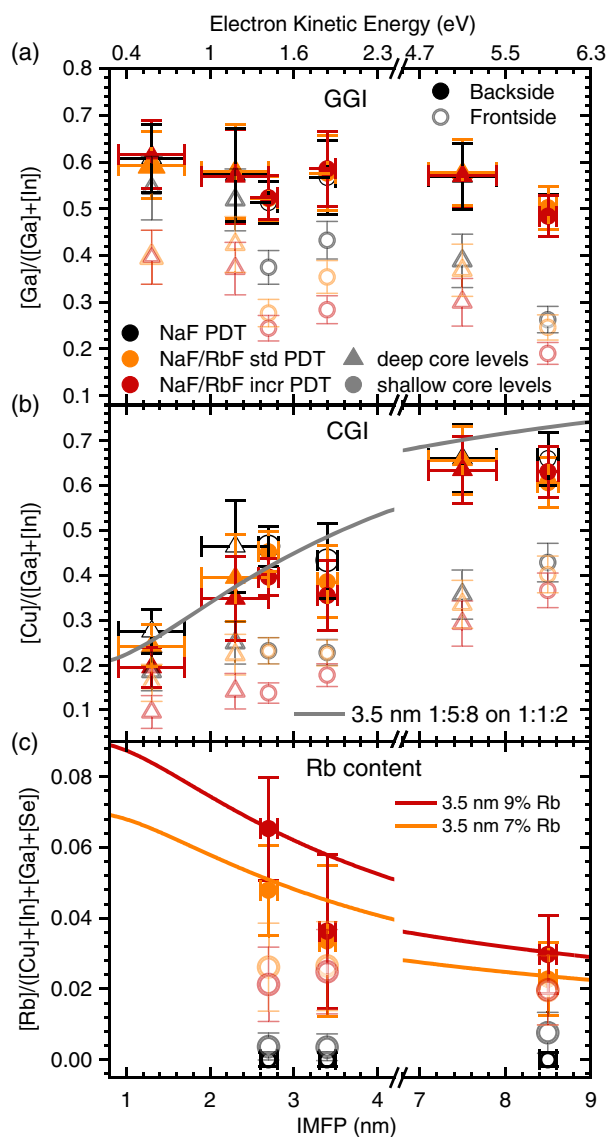
Figure 2. Surface composition of CIGSe backside samples, stripped off their substrates after undergoing a NaF, NaF/RbF std, and NaF/RbF incr PDT as a function of IMFP, determined from spectra measured with 1.3 keV (Mg K_α), 2 keV, and 6 keV. a) [Ga]/([Ga]+[In]) as a measure of Ga content. b) [Cu]/([Ga]+[In]) ratio as a measure of Cu content. The gray solid line represents a simple bilayer model of a 3.5 nm-thick 1:5:8 CIGSe phase on top of a stoichiometric 1:1:2 CIGSe. c) [Rb]/([Cu]+[In]+[Ga]+[Se]) ratio as a measure of Rb content. The lines represent a model in which Rb is only present in the 3.5 nm-thick 1:5:8 CIGSe layer with Rb concentrations of 7% (orange line) and 9% (red line) on top of a Rb-free 1:1:2 CIGSe phase. For the Cu and Ga ratios (a,b), shallow (In 4d, Ga 3d, Cu 3p) and deep (In 3p, Ga 2p, and Cu 2p) core levels were used, resulting in IMFPs of 8.5, 3.4, 2.7 (shallow core levels) and 7.5, 2.3, and 1.3 nm (deep core levels). For the ratios shown in panel c) only the shallow core-level data were used. Corresponding data of the CIGSe frontside of the respective samples is displayed in panel (a–c) by semitransparent open symbols. Note that the Rb/CIGSe data of the frontside only correspond to Rb in the same chemical environment as at the backside and ignore Rb in the form of a Rb—In—Se-type species.[11]

back gradient.[27] In contrast, the pronounced CGI decrease for lower IMFPs indicates a Cu depletion at the back surface (compared with a CGI = 1 expected for a [Cu]:([In]+[Ga]):[Se] = 1:1:2 CIGSe stoichiometry), similar to previous results for the CIGSe frontside of these samples.[11] However, the Cu depletion at the backside seems to be confined to a thin, more superficial region in contrast to the frontside, where low CGI values are also seen for measurements with higher IMFPs. It is, however, not certain whether the absorber backside is inherently Cu-poor or whether the Cu depletion is induced by the cleavage of the CIGSe/Mo interface upon stripping, potentially causing a surface reconstruction of the CIGSe backside. However, we can reasonably explain the data (see gray line in Figure 2b)) with a model that assumes a 3.5 ($\pm$1.0) nm thick layer of a [Cu]:([In]+[Ga]):[Se] = 1:5:8 phase on stoichiometric 1:1:2 CIGSe. While the increasing discrepancy between this simple bilayer model and the data points with increasing IMFP can be explained by the limitation of the applied quantification approach (see Experimental Section), a more complex scenario including a Cu gradient is also possible. While the GGI at the backside is not influenced by the application of a NaF/RbF PDT, a slight (i.e., within the error bar but systematic) decrease in CGI scaling with the Rb amount during PDT is detected.

The Rb content (i.e., the [Rb]/([Cu]+[In]+[Ga]+[Se]) ratio shown in Figure 2c) is significantly increased toward low IMFPs, indicating an accumulation of Rb at the absorber back surface. When comparing it with the amount of the corresponding Rb species at the frontside, attributed to Rb incorporated in the Cu-deficient CIGSe surface region,[11] we see a much higher Rb concentration at the backside for low IMFP data. However, when comparing the most bulk-sensitive HAXPES measurements, which best reflect the overall Rb content in the (extended) near-surface region due to their larger information depth (see Experimental Section), we see a similar [Rb]/([Cu]+[In]+[Ga]+[Se]) ratio. From this, we can conclude a roughly similar amount of this Rb species in the near-surface bulk region at the CIGSe front and backside, which is, however, significantly more concentrated toward the very surface at the backside. Considering the obtained CGI depth profile, we modeled the [Rb]/([Cu]+[In]+[Ga]+[Se]) data using formula (1) (see red and orange lines in Figure 2c)), assuming that Rb is homogeneously distributed in the suggested 3.5 nm-thick Cu-poor 1:5:8 surface region. This modeling leads to Rb concentrations of 7($\pm$1.5)% (NaF/RbF std PDT) and 9($\pm$2)% (NaF/RbF incr PDT) inside this layer.

Apart from the CIGSe backside samples, the survey spectra of the Mo side (Figure S15, Supporting Information) obtained by stripping the CIGSe absorbers off are also measured. The spectra show pronounced signals from Mo and Se in accordance with the known presence of a Mo—Se phase on Mo back contacts.[19,28,29] The present O 1s and C 1s signals are attributed to surface adsorbates. On the Mo-side sample of the NaF/RbF std process measured with 6 keV, a F 1s signal can be detected which we contribute to a contamination during sample preparation, transport, storage, or mounting and assume to be negligible for the following considerations due to its low intensity. By zooming in

the vertical scale of the survey spectra, spectral intensity related to the most prominent Cu, In, and Ga lines can be found (Figure S16, Supporting Information). To investigate whether this could be related to small CIGSe crystallites that remained at the Mo side, we calculated the stoichiometry by means of the GGI and Cu/In ratios and displayed them in **Figure 3**a. While the Cu/In ratio is similar at the Mo side and CIGSe backside, the GGI as a measure of relative Ga content increases significantly at the Mo side. This is in agreement with previous observations, suggesting the incorporation of Ga into the top region of the Mo side.[19]

For a more detailed analysis of the Mo-side chemical environment, we fitted the Se 3d and Mo 4p core-level spectra (Figure S17, Supporting Information) and calculated the Mo/Se ratios, which (considering the experimental uncertainty) reasonably agree with the formation of a $MoSe_2$ phase independent of performed PDTs.[19,28,29] As both Se 3d and Mo 4p spectra can be fitted using a single component, we exclude the presence of a significant amount of additional Mo- or Se-containing phases. However, for measurements with higher excitation energy and correspondingly larger IMFP, a pronounced Fermi edge in the measured valence band spectra is detected (Figure S18d, Supporting Information), indicating the presence of a metallic

species, which we attribute to metallic Mo underneath the $MoSe_2$.[28–30]

Apart from the pronounced Mo and Se contributions on the Mo surfaces, we also find a small but significant Rb signal for the samples undergoing the NaF/RbF PDTs. The spectra and fits of the Rb 3d peak are shown in Figure 3b. By comparing Rb/In ratios of the CIGSe backside and respective Mo-side samples, we find that this Rb is not present as part of a chalcopyrite remnant which was not removed by the stripping process (see SI section "Rb at Mo side" including Figure S19, Supporting Information, for detailed discussion). Therefore, we conclude that some Rb either diffuses into the $MoSe_2$ (e.g., intercalating into the interlamellar gaps of the layered van der Waals material $MoSe_2$) or accumulates at its surface. Depth-dependent HAXPES measurements (see Figure S20, Supporting Information) rather support the latter.

To investigate the energy-level alignment at the back interface, we determined the valence band maxima (VBM) position of the CIGSe backside and the respective Mo-side samples by linear extrapolation of the leading edge of the valence band photoemission spectra (Figure S18, Supporting Information) and displayed them in **Figure 4** alongside the previously reported IMFP-dependent VBM values of the corresponding CIGSe frontsides.[11] Similar to what is commonly seen at the CIGSe frontside,[11,13] an IMFP-dependent shift of the VBM away from the Fermi level (E_F) is also visible at the backside. While in the cases of NaF and NaF/RbF std treatments, the VBM values measured at the backsides with high surface sensitivity (ultraviolet photoelectron spectroscopy [UPS]) are consistent with previously published data[20] (depicted as gray dotted lines in Figure 4a), we detect a small downward shift in the case of the NaF/RbF incr case. A similar shift of the VBM at the surface as a cause of NaF/RbF PDT was also found at the frontside of the samples. To discuss this shift, we depict the respective valence band spectra of the CIGSe backside samples in Figure 4d: while the NaF-treated sample shows a significant feature attributed to antibonding Se d–Cu p states[31] between 1 and 2 eV in binding energy, this feature is reduced in the NaF/RbF PDT samples. This reduction is more pronounced in the NaF/RbF incr case, leading to a shift of the VBM away from E_F. The intensity decrease in this Cu-related feature agrees well with the Rb-correlated, enhanced Cu depletion at the CIGSe backside that was discussed earlier.

Similar to the absorber backside, the VBM seen on the Mo side agree very well with previous work.[20] At the surface of the Mo side, mainly probing the $MoSe_2$ by UPS, we find a VBM of (-0.83 ± 0.10) eV relative to E_F, independent of the type of PDT. HAXPES measurements with a higher IMFP show a Fermi edge from the underlying metallic Mo (see Figure S18d, Supporting Information), as shown in Figure 4. These results provide an approximate picture of the energy level alignment at the CIGSe/Mo interface because it neglects the electronic interactions that may result in interface-induced band bending when the layers are in direct contact. Based only on the VBM determined by UPS (IMFP < 1 nm) of the two (i.e., CIGSe backside and Mo side) exposed surfaces, no VBM offset between both layers would be expected, which would result in a good hole extraction across the interface, in agreement with the high power conversion efficiencies reported for these solar cell devices. The small VBM shift away from the Fermi level at the CIGSe backside
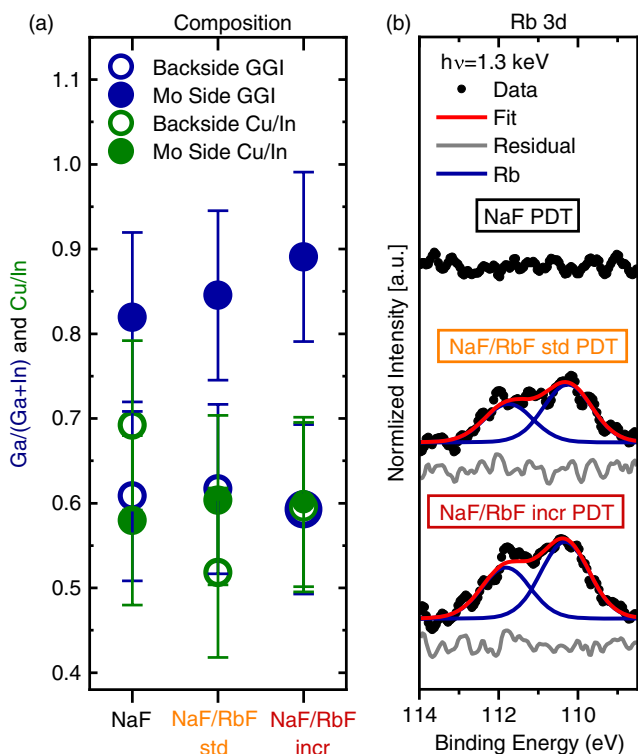

Figure 3. a) Cu, In, and Ga composition of CIGSe backside and respective Mo-side samples displayed as [Ga]/([Ga]+[In]) (GGI) and [Cu]/[In] ratios; calculated from fits shown in Figure S12, Supporting Information (backside) and Figure S14, Supporting Information (Mo side). b) Mg K$_\alpha$ Rb 3d core-level spectra of the Mo side of the different PDT CIGSe samples. Data are shown with a linear background subtracted. Respective fits using pairs of Voigt profiles to represent the respective doublets are displayed along the data as well as the respective residuals.
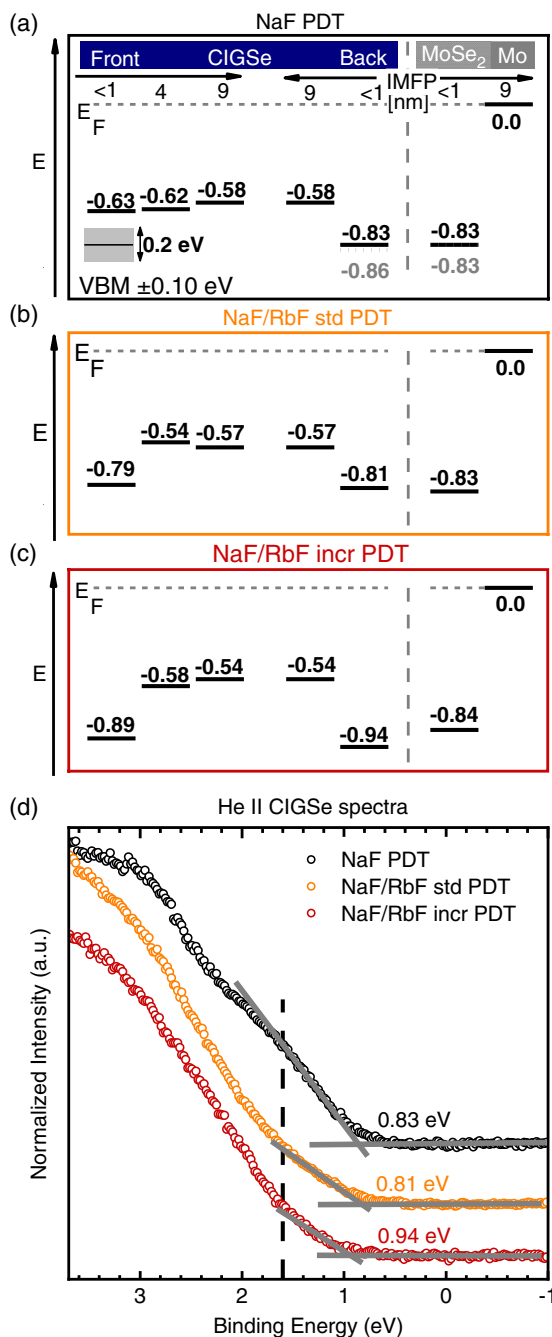
Figure 4. a–c) Energetic position of the VBM of CIGSe absorber backsides and their respective Mo-side counterparts as a function of IMFP, determined from spectra recorded with He II (40.8 eV), and 6 keV shown as solid black lines. Corresponding data of the CIGSe frontside of the respective samples are also displayed in panel (a–c).[11] The literature data[20] of a CIGSe absorber backside prepared without alkali PDT are shown as gray dotted lines in panel (a). The given error for all VBM values obtained in this contribution is ±0.1 eV. d) UPS spectra (He II) of the CIGSe absorber backside are displayed together with the used linear extrapolation visualized as gray dashed lines. A black dashed line marks the position of antibonding hybridized Se p–Cu d states according to Kuznetsova et al.[31]

induced by the excessive RbF treatment suggests the formation of a small VB discontinuity (≈0.1 eV) at the CIGSe/Mo interface, from which, however, no detrimental effects on the device efficiency would be expected.[32] The fact that we do not detect a relevant band offset at the back interface agrees with results of other studies, suggesting that the deteriorating effects of (over) pronounced RbF PDTs can be related to a barrier at the front (and not the back) interface of the CIGSe absorber.[18] In contrast to the well-aligned VB across the CIGSe/Mo(Se₂) interface, the CIGSe VBM derived from the more bulk-sensitive (IMFP = 9 nm) measurements indicate a VBM position much closer to E_F compared with the values derived from the more surface-sensitive (IMFP < 1 nm) measurements, indicating a pronounced downward band bending toward the CIGSe back surface. Such band bending would repel holes from the CIGSe/Mo(Se₂) interface and therefore be detrimental for charge extraction, which somewhat contradicts the fact that this configuration results in high-efficiency solar cells.[7] A possible explanation would require a highly efficient (lossless) tunnel-assisted charge carrier extraction across the back interface. However, as the experiment design and characterization approach do not allow the direct study of the chemical and electronic absorber/ substrate interface structure (but only provide information on the materials separated from each other), any effect due to, e.g., charge transfer and/or surface reconstruction is not considered and thus might impact this conclusion. Furthermore, the expected flattening of the downward band bending toward the absorber backside under operating conditions might also mitigate this issue.

3. Conclusion

The impact of combined NaF/RbF postdeposition treatments on the deeply buried CIGSe/Mo interface was studied by photoelectron spectroscopy and electron microscopy using a cleaving procedure, stripping the CIGSe absorbers from the substrates. We detect Cu depletion at the CIGSe backsides, which can be modeled as a 3.5 nm-thick Cu-deficient [Cu]:([In]+[Ga]):[Se]=1:5:8 layer on stoichiometric 1:1:2 CIGSe. In the case of a combined NaF/RbF PDT, we find a Rb enrichment at the CIGSe/Mo interface, which is associated with an enhancement of the Cu depletion at the CIGSe backside and to some extent with a VBM shift away from the Fermi level. While this is similar to what was found at the NaF/RbF PDT CIGSe front surface,[11] the main difference is the lack of the NaF/RbF PDT-induced formation of a Rb—In—Se-type compound. Rb is only present as a single species that is assigned to Rb incorporated into the Cu-deficient surface region of CIGSe, in agreement with our previous study of the CIGSe front surface. The absence of a Rb—In—Se-type compound at the CIGSe backside supports the suggestions that a (pronounced) Rb—In—Se layer (as found on the CIGSe front surface) can act as a charge transport barrier; in-line with the finding that such barriers observed for CIGSe devices PDTed with excessive amounts of RbF can be removed by etching of the front surface (removing the Rb—In—Se layer).[18] On the Mo side, we detected a thin layer of MoSe₂ and Rb at low concentrations.

**ADVANCED
SCIENCE NEWS**

www.advancedsciencenews.com

**ADVANCED
ENERGY & SUSTAINABILITY
RESEARCH**
Open Access

www.advenergysustres.com

The latter, however, does not appear to exhibit any major impact on the chemical (i.e., no formation of additional species) or electronic (i.e., unaffected VBM position) structures.

4. Experimental Section

Sample Preparation and Handling: The CIGSe samples were prepared at Empa using a low-temperature (i.e., substrate temperature during CIGSe deposition <500 °C, compatible with the use of, e.g., polyimide substrates) multistage process on Mo/SiO$_x$-coated SLG substrates. The silicon oxide acts as a diffusion barrier for alkali elements that would otherwise diffuse during absorber preparation (at elevated temperatures) from the SLG into the CIGSe. The CIGSe absorbers were then subject to alkali fluoride PDTs, i.e., evaporating NaF (samples referred to as "NaF PDT" in this work) or NaF followed by RbF in the presence of Se vapor. The two NaF/RbF PDT samples studied here had equivalent synthesis procedures, except for the differing RbF evaporation rates—and therefore total amounts of RbF added.[7] Samples to which the standard RbF evaporation rate (1–2 nm min^{-1}) was applied, which has previously been shown to lead to solar cell power conversion efficiencies above 19%, are referred to as "NaF/RbF std." Samples with an increased RbF evaporation rate (which was reported to lead to a deteriorated device performance, if processed into working cells[7]) will be here referred to as "NaF/RbF incr." Details about sample manufacturing and the PDT process can be found in Avancini et al.[7] After preparation, samples were sealed and packed at Empa, minimizing exposure to oxygen and moisture by extracting the samples from the evaporation vacuum chambers into nitrogen-filled glove bags. The samples were then double-bagged in inert nitrogen atmosphere and shipped to the HZB, where they were unpacked and mounted on suitable sample holders in a dry-N$_2$-filled glove box directly connected to the surface analysis system in the Energy Materials In Situ Laboratory Berlin (EMIL). After the characterization of the frontside (results can be found in Bombsch et al.[11]), the absorbers were stripped off their Mo back contacts: a stainless steel plate was glued to the CIGSe front surface using vacuum compatible silver epoxy glue. After curing the silver epoxy at room temperature for 24 h, the steel/CIGSe/Mo/SiO$_x$/glass sample was exposed to liquid nitrogen. In addition, mechanical force was applied in opposite directions to the stainless steel plate and the glass substrate. The resulting mechanical and thermal stress resulted in a cleavage mainly along the CIGSe/Mo plane. The stripped steel/CIGSe (referred to as "CIGSe backside" in this manuscript) and Mo/SiO$_x$/glass ("Mo side") samples were kept in liquid nitrogen for transfer into a dry-N$_2$-filled glove box, where the CIGSe back surface and Mo-side samples were mounted. Subsequently, the samples were directly transferred into the connected surface analysis system without air exposure. The samples were then characterized using laboratory-based UPS and X-ray photoelectron spectroscopy (XPS) as well as by synchrotron-based HAXPES at HZB's BESSY II facility (more details below). After initial spectroscopic analysis at HZB, the samples were mounted on suitable sample holders in ambient conditions (air exposure approximately 10 min) for complementary scanning electron microscopy (SEM)/EDX measurements. Additional HAXPES measurements using an excitation energy of 6 keV were performed at SPring-8. For these measurements, it was inevitable to expose the samples to air for about 2 h during mounting and introduction into the measurement system. Each of the three measurement sets (lab UPS/XPS, HAXPES at BESSY II, HAXPES at SPring-8) were performed on freshly stripped samples. The measured samples therefore represent different sections of larger samples from which they were cut. Given the overall high quality of the absorber material, we do not expect a significant influence of lateral inhomogeneity on the results.

SEM and EDX: The SEM imaging and EDX analyses were conducted using a Zeiss UltraPlus SEM equipped with an Ultim Extreme X-ray detector by Oxford Instruments. EDX elemental distribution maps were acquired at 7 kV and evaluated using the software suite AZtec.

Laboratory-Based Photoelectron Spectroscopy: Laboratory-based XPS and UPS measurements were conducted using nonmonochromatized Mg K$_\alpha$ (1253.56 eV, referred to as 1.3 keV in the article), Al K$_\alpha$ (1486.58 eV, referred to as 1.5 keV in the article), and He II (40.8 eV) radiation and a ScientaOmicron Argus CU electron analyzer. The pressure of the analysis chamber during the measurement was 5×10^{-9} mbar. The pass energy for the shallow core level and Auger line detail spectra measurements was set to 20 eV, resulting in a combined analyzer and excitation resolution of approximately 0.9 eV for Mg K$_\alpha$ and 1.2 eV for Al K$_\alpha$. For the UPS measurements using a He II light source, the pass energy was set to 4 eV resulting in a total combined resolution of approximately 100 meV. The binding energy of the XPS measurements was calibrated by referencing the Au 4$f_{7/2}$ peak of a grounded clean Au foil to the binding energy of 84.00 eV. For the UPS measurements, the binding energy was calibrated by referencing the E_F of a grounded, clean Au foil to the binding energy of 0.00 eV.

Synchrotron-Based Photoelectron Spectroscopy: HAXPES experiments were conducted at the HiKE end-station[33] located at the BESSY II KMC-1 bending magnet beamline[34] at HZB and at beamline BL15XU[35] of the SPring-8 electron storage ring. The base pressure in both end-stations was $<1 \times 10^{-8}$ mbar, and they are both equipped with a Scienta R4000 electron energy analyzer with similar geometrical setups for beamline and analyzer: horizontal linear polarized X-rays, with the direction of polarization normal to the analyzer entrance slit, near-normal emission from the sample. Spectra were recorded using calibrated photon energies of 2.003 keV (referred to as 2 keV from hereafter and in the article) at BESSY II and of 5.95 keV (referred to as 6 keV in article) at SPring-8 using in both cases the Si(111) crystal of the double-crystal monochromator for energy selection. In addition, the Si(333) channel-cut crystal was used for HAXPES at SPring-8 to reduce the X-ray excitation line width. A pass energy of 200 eV was used for all measurements, resulting in a combined analyzer plus excitation resolution of approximately 0.25 eV for all HAXPES spectra. The binding energy was calibrated by referencing the Au 4$f_{7/2}$ peak of a grounded clean Au foil to a binding energy of 84.00 eV.

Depth Dependence: The samples were characterized by photoelectron spectroscopy using different excitation energies (6, 2, and 1.5 keV [Al K$_\alpha$], 1.3 keV [Mg K$_\alpha$], and 40.8 eV [He II]). For CIGSe (assuming a bandgap in the vicinity of the surface—where it is expected to be wider than in the bulk—of 1.6 eV[36] and a density of 5.7 g cm^{-2}, resulting from a linear combination of the values for CuInSe$_2$ and CuGaSe$_2$ given in Gilbert[37]), this results in maximum IMFPs of photoelectrons ranging from 9 to less than 1 nm.[38] As a higher IMFP leads to electrons from deeper inside the sample being able to reach the surface without energy loss due to scattering, this allows nondestructive examination of the depth-dependent chemical and electronic structure of the differently treated absorber (back) surfaces. The ratio of electrons reaching the surface of the sample unscattered (I) against the overall excited electrons (I_0) decreases exponentially with the depth, x, from which they are excited, following the Lambert—Beer law: $\frac{I(x)}{I_0} = \exp(-x/\text{IMFP})$.

Model Fit: Core-level spectra were fitted using linear backgrounds and Voigt profiles, keeping—if more than one species is present—the interspecies distances of the contributions to one core-level constant for all excitation energies and keeping the shape of the Voigt identical for identical core levels and excitation energies. For core levels with a splitting due to spin—orbit coupling (i.e., all core levels with an azimuthal quantum number (l)>0), two Voigt profiles with a fixed distance and a fixed intensity ratio according to $\frac{1+2(l+1/2)}{1+2(l-1/2)}$ were used.[39]

Stoichiometry Calculation: For calculating the ratios, deep core levels (Ga 2p, Na 1s, Cu 2p, In 3p) were corrected by photoionization cross section, analyzer transmission function, and IMFP.[40] Shallow core levels (Rb 3d, Cu 3p, Na 2s, Se 3d, Ga 3d, and In 4d) were only corrected by photoionization cross section;[22,41] in this case, the kinetic energy of the respective photoelectrons is very similar, and thus any impact of differing IMFPs or of the analyzer transmission is negligible.

Calculations of Bilayer Models: If we assume a bilayer model with two differently composed layers of same density, we can calculate the overall stoichiometric ratio (R) between different elements (e.g., [Cu]/([Ga]+[In])), which is expected to result from comparison of the XPS/HAXPES data with

different IMFPs. For this, it is necessary to know the ratios of the two single layers (R_1, R_2), the thickness of the top layer (d), and the IMFP, which we assume to be the same in both layers (see Mönig et al.[42] for more details)

$$R = R_1\left(1 - \exp\left(\frac{-d}{IMFP}\right)\right) + R_2\exp\left(\frac{-d}{IMFP}\right) \tag{1}$$

However, this formula requires the denominator of the ratio (i.e., [Ga]+[In] in the case of a [Cu]/([Ga]+[In]) ratio (CGI)) to be the same in both layers. In scenarios where this is not fulfilled (e.g., in the case when modeling the CGI of a 1:5:8 = [Cu]:[In+Ga]:[Se] phase on stoichiometric CIGSe), Equation (1) might lead to a slight overestimation (if the denominator is larger in the bulk compared with the cover layer) or underestimation (in the opposite case) of the resulting ratio which is more pronounced for higher IMFPs.

Supporting Information

Supporting Information is available from the Wiley Online Library or from the author.

Conflict of Interest

The authors declare no conflict of interest.

Data Availability Statement

Research data are not shared.

[1] P. Reinhard, B. Bissig, F. Pianezzi, E. Avancini, H. Hagendorfer, D. Keller, P. Fuchs, M. Döbeli, C. Vigo, P. Crivelli, S. Nishiwaki, S. Buecheler, A. N. Tiwari, *Chem. Mater.* **2015**, *27*, 5755.

[2] A. Chirilă, P. Reinhard, F. Pianezzi, P. Bloesch, A. R. Uhl, C. Fella, L. Kranz, D. Keller, C. Gretener, H. Hagendorfer, D. Jaeger, R. Erni, S. Nishiwaki, S. Buecheler, A. N. Tiwari, *Nat. Mater.* **2013**, *12*, 1107.

[3] T. Kodalle, M. D. Heinemann, D. Greiner, H. A. Yetkin, M. Klupsch, C. Li, P. A. van Aken, I. Lauermann, R. Schlatmann, C. A. Kaufmann, *Solar RRL* **2018**, *0*, 1800156.

[4] P. Jackson, R. Wuerz, D. Hariskos, E. Lotter, W. Witte, M. Powalla, *Phys. Status Solidi RRL* **2016**, *10*, 583.

[5] M. Nakamura, K. Yamaguchi, Y. Kimoto, Y. Yasaki, T. Kato, H. Sugimoto, *IEEE J. Photovolt.* **2019**, *9*, 1863.

[6] Solar Frontier Hits New CIS Cell Efficiency Record, https://www.pv-magazine.com/2019/01/21/solar-frontier-hits-new-cis-cell-efficiency-record/ (accessed: July 2021).

[7] E. Avancini, R. Carron, T. P. Weiss, C. Andres, M. Bürki, C. Schreiner, R. Figi, Y. E. Romanyuk, S. Buecheler, A. N. Tiwari, *Chem. Mater.* **2017**, *29*, 9695.

[8] S. Siebentritt, E. Avancini, M. Bär, J. Bombsch, E. Bourgeois, S. Buecheler, R. Carron, C. Castro, S. Duguay, R. Félix, E. Handick, D. Hariskos, V. Havu, P. Jackson, H.-P. Komsa, T. Kunze, M. Malitckaya, R. Menozzi, M. Nesladek, N. Nicoara, M. Puska, M. Raghuwanshi, P. Pareige, S. Sadewasser, G. Sozzi, A. N. Tiwari, S. Ueda, A. Vilalta-Clemente, T. P. Weiss, F. Werner, et al., *Adv. Energy Mater.* **2020**, *10*, 1903752.

[9] C. P. Muzzillo, *Sol. Energy Mater. Sol. Cells* **2017**, *172*, 18.

[10] E. Handick, P. Reinhard, R. G. Wilks, F. Pianezzi, T. Kunze, D. Kreikemeyer-Lorenzo, L. Weinhardt, M. Blum, W. Yang, M. Gorgoi, E. Ikenaga, D. Gerlach, S. Ueda, Y. Yamashita, T. Chikyow, C. Heske, S. Buecheler, A. N. Tiwari, M. Bär, *ACS Appl. Mater. Interfaces* **2017**, *9*, 3581.

[11] J. Bombsch, E. Avancini, R. Carron, E. Handick, R. Garcia-Diez, C. Hartmann, R. Félix, S. Ueda, R. G. Wilks, M. Bär, *ACS Appl. Mater. Interfaces* **2020**, *12*, 34941.

[12] N. Taguchi, S. Tanaka, S. Ishizuka, *Appl. Phys. Lett.* **2018**, *113*, 113903.

[13] E. Handick, P. Reinhard, J.-H. Alsmeier, L. Köhler, F. Pianezzi, S. Krause, M. Gorgoi, E. Ikenaga, N. Koch, R. G. Wilks, S. Buecheler, A. N. Tiwari, M. Bär, *ACS Appl. Mater. Interfaces* **2015**, *7*, 27414.

[14] D. Hauschild, D. Kreikemeyer-Lorenzo, P. Jackson, T. M. Friedlmeier, D. Hariskos, F. Reinert, M. Powalla, C. Heske, L. Weinhardt, *ACS Energy Lett.* **2017**, *2*, 2383.

[15] R. Wuerz, W. Hempel, P. Jackson, *J. Appl. Phys.* **2018**, *124*, 165305.

[16] A. Vilalta-Clemente, M. Raghuwanshi, S. Duguay, C. Castro, E. Cadel, P. Pareige, P. Jackson, R. Wuerz, D. Hariskos, W. Witte, *Appl. Phys. Lett.* **2018**, *112*, 103105.

[17] P. Schöppe, S. Schönherr, P. Jackson, R. Wuerz, W. Wisniewski, M. Ritzer, M. Zapf, A. Johannes, C. Schnohr, C. Ronning, *ACS Appl. Mater. Interfaces* **2018**, *47*, 40592.

[18] T. P. Weiss, S. Nishiwaki, B. Bissig, R. Carron, E. Avancini, J. Löckinger, S. Buecheler, A. N. Tiwari, *Adv. Mater. Interfaces* **2018**, *5*, 1701007.

[19] M. Bär, L. Weinhardt, C. Heske, S. Nishiwaki, W. N. Shafarman, *Phys. Rev. B* **2008**, *78*, 075404.

[20] M. Bär, S. Nishiwaki, L. Weinhardt, S. Pookpanratana, W. N. Shafarman, C. Heske, *Appl. Phys. Lett.* **2008**, *93*, 042110.

[21] L. Weinhardt, M. Blum, M. Bär, C. Heske, O. Fuchs, E. Umbach, J. D. Denlinger, K. Ramanathan, R. Noufi, *Thin Solid Films* **2007**, *515*, 6119.

[22] M. B. Trzhaskovskaya, V. I. Nefedov, V. G. Yarzhemsky, *At. Data Nucl. Data Tables* **2001**, *77*, 97.

[23] O. Keski-Rahkonen, M. O. Krause, *At. Data Nucl. Data Tables* **1974**, *14*, 139.

[24] A. J. Nelson, S. Gebhard, L. L. Kazmerski, E. Colavita, M. Engelhardt, H. Höchst, *Appl. Phys. Lett.* **1990**, *57*, 1428.

[25] M. Chugh, T. D. Kühne, H. Mirhosseini, *ACS Appl. Mater. Interfaces* **2019**, *11*, 14821.

[26] R. K. M. Raghupathy, T. D. Kühne, G. Henkelman, H. Mirhosseini, *Adv. Theory Simul.* **2019**, *2*, 1900036.

[27] E. Avancini, R. Carron, B. Bissig, P. Reinhard, R. Menozzi, G. Sozzi, S. D. Napoli, T. Feurer, S. Nishiwaki, S. Buecheler, A. N. Tiwari, *Progr. Photovolt. Res. Appl.* **2017**, *25*, 233.

[28] T. Glatzel, D. F. Marrón, T. Schedel-Niedrig, S. Sadewasser, M. C. Lux-Steiner, *Appl. Phys. Lett.* **2002**, *81*, 2017.

[29] T. Wada, N. Kohara, S. Nishiwaki, T. Negami, *Thin Solid Films* **2001**, *387*, 118.

[30] D. Abou-Ras, G. Kostorz, D. Bremaud, M. Kälin, F. V. Kurdesau, A. N. Tiwari, M. Döbeli, *Thin Solid Films* **2005**, *480–481*, 433.

[31] T. V. Kuznetsova, V. I. Grebennikov, H. Zhao, C. Derks, C. Taubitz, M. Neumann, C. Persson, M. V. Kuznetsov, I. V. Bodnar, R. W. Martin, M. V. Yakushev, *Appl. Phys. Lett.* **2012**, *101*, 111607.

[32] T. Minemoto, T. Matsui, H. Takakura, Y. Hamakawa, T. Negami, Y. Hashimoto, T. Uenoyama, M. Kitagawa, *Sol. Energy Mater. Sol. Cells* **2001**, *67*, 83.

[33] M. Gorgoi, S. Svensson, F. Schäfers, G. Öhrwall, M. Mertin, P. Bressler, O. Karis, H. Siegbahn, A. Sandell, H. Rensmo, W. Doherty, C. Jung, W. Braun, W. Eberhardt, *Nucl. Instrum. Methods Phys. Res.* **2009**, *601*, 48.

[34] F. Schaefers, M. Mertin, M. Gorgoi, *Rev. Sci. Instrum.* **2007**, *78*, 123102.

[35] S. Ueda, Y. Katsuya, M. Tanaka, H. Yoshikawa, Y. Yamashita, S. Ishimaru, Y. Matsushita, K. Kobayashi, *AIP Conf. Proc.* **2010**, *1234*, 403.

[36] M. Bär, S. Nishiwaki, L. Weinhardt, S. Pookpanratana, O. Fuchs, M. Blum, W. Yang, J. D. Denlinger, W. N. Shafarman, C. Heske, *Appl. Phys. Lett.* **2008**, *93*, 244103.

[37] B. Gilbert, *Isr. J. Chem.* **1965**, *3*, 120.

[38] S. Tanuma, C. J. Powell, D. R. Penn, *Surf. Interface Anal.* **1994**, *21*, 165.

[39] F. de Groot, A. Kotani, in *Core Level Spectroscopy of Solids* (Ed: D.D. Sarma), CRC Press, Boca Raton, FL **2008**, p. 13, 14, 97, 98.

[40] S. Tanuma, C. J. Powell, D. R. Penn, *Surf. Interface Anal.* **1993**, *20*, 77.

[41] M. B. Trzhaskovskaya, V. K. Nikulin, V. I. Nefedov, V. G. Yarzhemsky, *At. Data Nucl. Data Tables* **2006**, *92*, 245.

[42] H. Mönig, C.-H. Fischer, R. Caballero, C. A. Kaufmann, N. Allsop, M. Gorgoi, R. Klenk, H.-W. Schock, S. Lehmann, M. C. Lux-Steiner, I. Lauermann, *Acta Mater.* **2009**, *57*, 3645.